Machine Learning Based Hydro-mechanic Modeling for Sailing Commercial Ships

Nico van der Kolk*

Blue Wasp Marine
nvanderkolk@bluewaspmarine.com

Brian S. Freeman

Lakes Environmental
brian.freeman@weblakes.com

Abstract

The maturity of Reynolds-averaged Navier Stokes computational fluid dynamics (RANS-CFD) packages offers the ready assessment of the hydro-mechanic performance of a wind-assisted commercial ship. However, these simulations require intensive computational resources and complex software to generate results. In the hull optimisation context, individual adjustments to parameters require discrete processing that may take hours or days to process. To expedite results under different hull designs, or in the context of bulk analysis of multiple vessels in a fleet, machine learning models are trained on a database of RANS-CFD for a systematic hull series. The model successfully reproduced the RANS-CFD results with over 98% accuracy for 60 different hull variations and allowed for rapid, accurate reporoduction of vessel response for generic wind-assist hulls which can be quickly evaluated under a wide variety of sailing conditions.

I. Introduction

Wind assisted ship propulsion stands apart among available technologies for the energy transition in commercial shipping. A wind-hybrid vessel promises to deliver substantial fuel savings, a result that has been reported by several researchers in recent years [8, 20, 28, 6]. This promise of substantial reductions in emissions, for both local pollutants and for greenhouse gases, is achievable in the near-term.

Technological readiness of wind assist concepts is not the barrier to broader market uptake. Several viable concepts for wind propulsors are commercially available. Rather, it is a lack of experience with industrialized sailing and unwillingness to take risk as an 'early adopter'. The further development of this promising technology is hampered by a poor understanding of the interaction effects between wind propulsors and the hydro-mechanics of commercial ships. For the ship owner or operator, this lack of experience with industrial sailing introduces uncertainty in a profoundly risk-averse sector. For the regulator who wishes to promote the uptake of sustainable technologies, the knowledge gap raises the spectre of misdirected policies that fail to advance wind assisted ship propulsion as a viable component of the energy transition. In fact, wind propulsion is one of the only interventions in the maritime shipping sector that promises significant reductions in greenhouse gas emissions in the near term. Furthermore, besides the simple arithmetic of fuel savings and limiting exposure to increasingly volatile fuel prices, wind-assistance raises the possibility of engaging with an activist consumer class and potentially increasing the perceived value of shipped products.
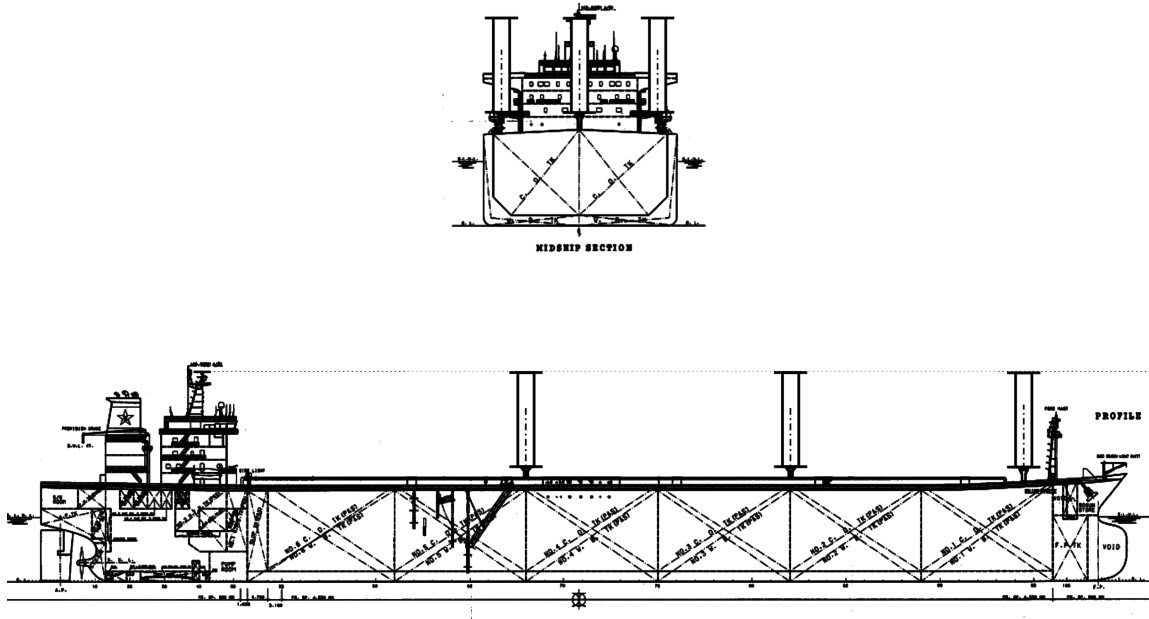
---

*Corresponding author

Figure 1: *80,000 DWT Panamax bulker with three 30-meter Flettner rotors.*

i.   Wind-assist vessel model

The reliable performance prediction of a wind-assisted ship is a necessary prerequisite for any sound economic and environmental evaluation of these concepts. Recognizing a general lack of understanding about the physics of wind-assist vessels, and the need for an assessment tool to facilitate the further development of this promising technology, a performance prediction tool is being developed by the Sail Assist research group. A quick yet reliable way to assess the performance of different wind-assisted ships will be useful throughout the design process. In early stages, when the user wants to explore several different designs, the in-built force models under development at Delft University of Technology may be used. In a more advanced design phase, the user can input data obtained by dedicated simulations or experiments. In this case the modeling tool is used purely as a solver to obtain very detailed results for a specific design.

The fundamental task of the performance prediction tool is to balance the aerodynamic and hydrodynamic forces acting on a wind-assisted ship to arrive at a sailing equilibrium. This is done within an optimization routine using the available wind-assist power, P_{WASP}, defined as:

$$P_{\text{WASP}} = \frac{V_{\text{ref}}}{\eta_{\text{T}}} \left(X_{\text{Aero}} - \Delta R_{\text{Sailing}} \right) - \frac{P_{\text{Rotor}}}{\eta_{\text{Gen}}} \tag{1}$$

This performance metric considers the wind-assist propulsive power against any power needed to operate the wind propulsor. The program calculates the performance of the wind-assisted ship for a specified range of true wind angle and true wind speed. A design can be evaluated and improved based on this modeling, or this information can be passed to a weather routing program or used to define the control systems of the wind propulsor. Finally, vessel performance with wind assist operation can be optimized, and studied for environmental impact and economic investment evaluations.

The sailing performance for wind-assisted ships is synonymous with maneuvering forces for the steady drift condition, including ves-

sel heel angle. A right hand rule is adopted with the z axis pointed down. All rotations are performed about midship at the calm water line. Forces and moments are presented in flow-aligned coordinates, $< x, y >$, with the suitable transformation as in Figure 2.
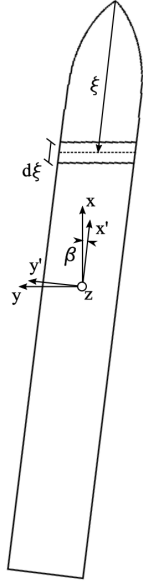

Figure 2: *Coordinate system for vessel hydro-mechanic response (viewpoint is below the ship).*

A linear and third order term are assumed for β, and a linear term for heel angle ϕ.

$$C_X = X_{\beta\beta}\beta^2 + X_\phi\phi \tag{2a}$$

$$C_Y = Y_\beta\beta + Y_{\beta\beta\beta}\beta^3 + Y_\phi\phi \tag{2b}$$

$$C_N = N_\beta\beta + N_\phi\phi \tag{2c}$$

The estimation of the hydrodynamic derivatives, $X_{\beta\beta}$, X_ϕ, Y_β, $Y_{\beta\beta\beta}$, Y_ϕ, N_β, and N_ϕ follows from analysis of results from the database of full-scale simulation results, as described in [31, 30], for the DWA. This approach to vessel modeling follows the same methodology as Tsakonas [29], Jacobs [15], Inoue et al. [14], Keuning and Sonnenberg [17], Toxopeus [27], in the maneuvering and sailing fields.

II. Methodology

i. Modeling for hydro-mechanic response

The ship adopts a heel and leeway angle to support the sail-plan. This combination places the hull—which is otherwise optimized for quite specific and symmetric operating conditions—oblique to the mean flow in the *sailing condition*.

An example of the vessel wave system and transverse hydrodynamic force is plotted in Figure 3. The normal wave field produced as part of the wake of this ship will be superimposed on the pressure distribution arising from the sideforce production by the hull, along with the Munk yawing moment [18]. Finally, a vessel heeling angle will bring the vessel "shoulders" closer to the free surface, leading to a further distortion of the wave system. The pressure resistance for a sailing ship will therefore vary with heel and leeway angles, alongside the ordinary Froude number dependency.

i.1 Sailing efficiency

Under the analysis of sailing yachts by Gerritsma and Keuning [10], the resistance increase due to sideforce production is modeled as an effective draft, T_e [11], which is a metric for the sailing efficiency of the hull. The expression is derived from the lifting-line theory of wings. This related to the slope of a linear fit through data for several heel and leeway angles. Following theories for low-aspect planforms [13, 16], this induced drag may be significant for commercial ships, meaning that the thrust delivered by a wind propulsor might well be overwhelmed by this increase in resistance. Though the flow mechanisms only vaguely resemble the Prandtl lifting-line and the associated derivation for the induced drag [22], the accounting for energy loss in shed vorticity is especially relevant for the present
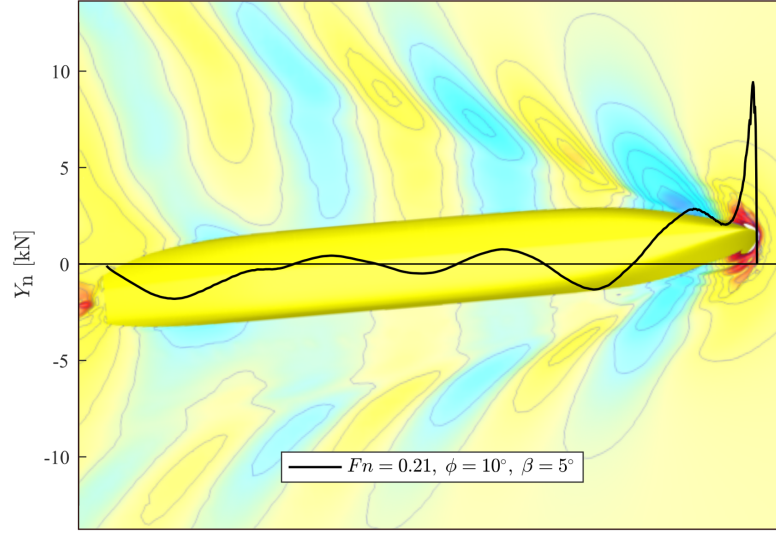
Figure 3: *Distribution of hydrodynamic sideforce, showing wave system (viewpoint is below the ship). Hull # 1, leeway angle $\beta = 5°$, heel angle $\phi = 10°$. As the vessel heels, the fore and aft shoulders are brought close to the free surface, causing flow constriction and acceleration. This effect is especially pronounced at large heel angles (ϕ=10° is normally adopted as operational limit for manned vessels).*

application. In non-dimensional form:

$$C_X = \frac{1}{\pi AR_{\text{eff}}} C_Y^2 + C_{XO} \tag{3a}$$

$$T_e = \sqrt{\frac{TLAR_{\text{eff}}}{2}} \tag{3b}$$

Forces and moments are non-dimensionalized using the dynamic pressure $q = \frac{1}{2}\rho U^2$ following the maneuvering convention. The AR_{eff}, as in Equation (3a) is derived from a (linear) curve fit. A non-dimensional form for the effective draft T_e is made with the vessel draft: T_e/T Equation (3b), providing a convenient metric for the sailing efficiency of the hull. Some difficulty arises on account of the non-linear response of the commercial ship hull.

i.2   Vessel course keeping ability

A second quantity of principal interest for this modeling for wind-assist vessels is the center of effort for the distribution of lateral force, also known as the center of lateral resistance. The position of the *CLR* is determined as the quotient of the yaw moment and the sideforce.

$$CLR = C_N/C_Y \tag{4}$$

Again, body forces are non-dimensionalized with the dynamic pressure q.

Behavior for the *CLR* as function of leeway angle β is shown in Figure 4 for several appendage configurations: the bare hull (un-appended), the nominal appended hull design with rudder set for zero degrees, a short bilge keel in the most forward position, and a long bilge keel occupying the full length of the parallel midbody. The *CLR* is given for leeway angles β of three, six, and nine degrees.
First, observe the *CLR* for the un-appended hull, which lies more than half a ships-length ahead of the bow (shown only for nine degrees leeway), a consequence of the stronger development of the yawing moment—linear with leeway angle—compared against the sideforce, which includes a significant higher-order dependency for leeway angle. The *CLR* moves aft as the leeway angle increases, an effect that is driven by an increase in flow separation along the bilges. This effect is manifest as a rising contribution for the higher-order sideforce term in the sway equation, and an attenuation
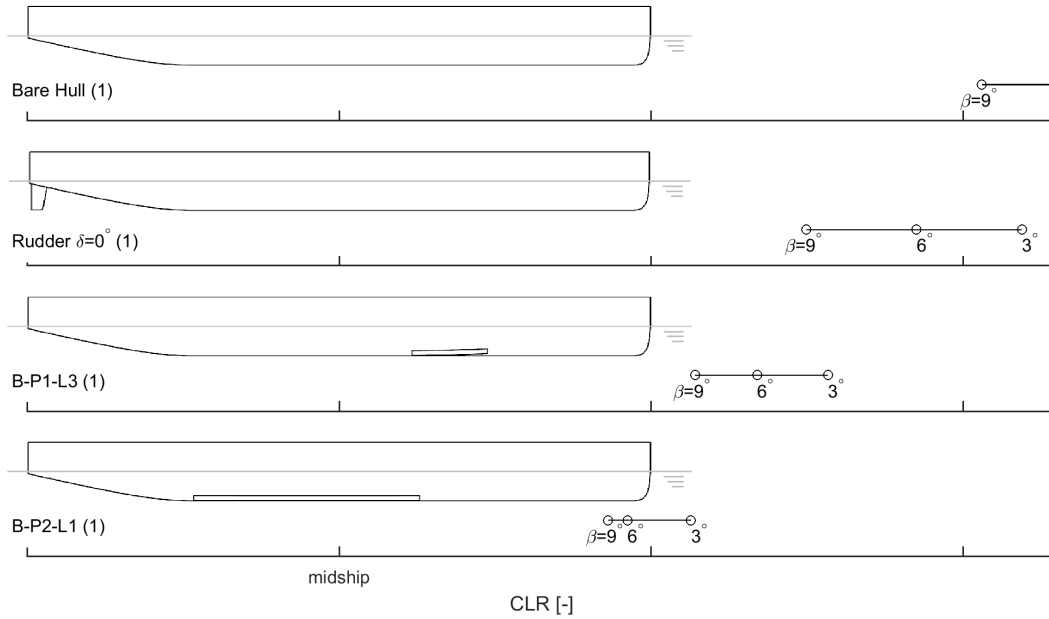
Figure 4: *Vessel CLR for several appended hulls. Experimental result.*

of the Munk moment for the yaw equation by flow separation along the vessel aft-body. Yaw balance, achieved by aligning the aerodynamic center of the wind propulsors with the hydrodynamic center (*CLR*) of the hull [2], is impossible.

i.3 Reynolds-averaged Navier Stokes simulation

Reynolds-averaged Navier Stokes computational fluid dynamics (RANS-CFD) and other numerical modeling packages are often used during the development of performance predictions for commercial ships to estimate sailing performance [26, 6, 31]. These methods require intensive computational resources and complex software to generate results, thereby limiting the number of scenarios, hull variations, and operating conditions a specific design can be evaluated under. Also, the computational effort may exceed what is appropriate under varying modeling contexts; i.e. global energy spectra analysis using database of operating vessels as under scenario analyses, or specific hull optimization routines. Reliable performance predictions are essential in new ship design and when considering modifications to existing hulls in order to improve operability and sailing efficiency.

A full scale simulation method is adopted to resolve essential Reynolds scaling difficulties, as described in [30]. The full-scale simulation method for the production runs is designed for the assessment of hull geometry variants of the Delft Wind-Assist Series, an extensive series of wind-assist ship hulls. Considering the volume of work, to be done at full scale, a premium must be placed on economical simulations–precluding near-wall modeling or elaborate turbulence models. The RANS equations are solved with the ISIS-CFD flow solver, developed at École Centrale Nantes and commercialized by Numeca International. The ISIS-CFD flow solver is an in-compressible unsteady RANS method. The unstructured spatial discretization for the transport equations is based on the finite volume method. Free-surface flows are simulated with a conservation equation for the mass fraction. A detailed description of the solver is provided in

[3, 4, 23, 5].

It is understood that flow around the hull will include large anisotropic vortices that will play a key role in the sailing performance of the hull. Turbulence is modeled with the Explicit Algebraic Stress Model (EASM), providing a balance between the Boussinesq-modeling and the modeling of Reynolds stresses and giving a more physical approach while remaining viable within the scope of work and for the computational resources available. The evaluation of convective terms in the momentum equation and the turbulent stresses is performed with a blended upwind/central scheme based on the local Courant number (Co). The solution for the free surface is determined following the volume of fluid method using an interface compression algorithm that is likewise dependent on the local Courant number. Complete documentation of the ISIS-CFD (FINE/Marine) solver is available [21]. Production simulation work was carried out at the Netherlands high performance computing cluster [1].

ii. Numerical modeling with machine learning

Machine learning is a generic term that covers a broad range of analytical processes including linear regression. Machine learning uses datasets to train software to recognize patterns or predict outcomes by updating parameters within an algorithm that minimizes the error associated with the data. The error could be the difference between the expected output versus the calculated output or simply be the shortest distance between a set of point. The most common type of machine learning algorithms use supervised learning (SL) in which input data is labeled with the expected output. The algorithm, or network, is repeated trained with the input data until the output error is small enough.

The basic unit of machine learning is a node as shown in Figure 5. The canonical FFNN model consists of an input layer, a hidden layer and an output layer. Each layer
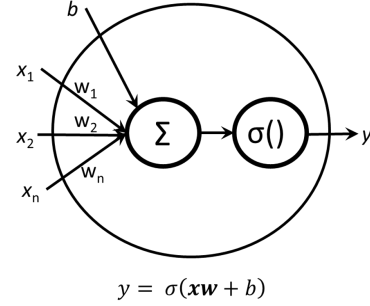

$$y = \sigma(xw + b)$$

Figure 5: *Basic node used in most machine learning architectures*

is constructed from interlinked nodes that generates a value (usually between -1 and 1 or 0 and 1). The individual node model is shown in Figure 5.

The node is based on the biologial neuron, where dendrites bring in sensory information in the form of bioelectric impulses until the neuron activates and sends another signal through its outputs. The machine learning node is similar to an individual neuron in that it also sums the weighted inputs of the previous layer, sometimes with a bias, and transforms the combined sum with a non-linear activation function, σ before producing an output that becomes the input to other nodes or an output itself. The node equation is given by

$$y = \sigma(wx + b) \tag{5}$$

where w is an array of weights for the connections between the previous layer and the current layer, x is a vector of input values from the previous layer, and b is an optional bias value. Common activation functions include the sigmoid, tanh, and relu functions. A general property for activation functions is that they normalize the output and have a continuous first order derivative that can be used during the training process [12].

When many, or thousands, of nodes are used in a machine learning architecture, they become an artificial neural network (ANN). Because of the complex interconnections and

nonlinear activation functions, ANNs have been successfully used to approximate complex functions and are often called 'universal approximators' [24, 25]. The basic ANN is a feed-forward neural network (FFNN) as shown in Figure 6. It includes an input layer that takes the input data features and distributes it to hidden layers for processing. The hidden layers due the bulk of the ANN calculations because of the interconnections between nodes. Each interconnection has a weight that can be updated or turned off. An output layer converts the final calculations into a binary category or a continuous value that may require further re-mapping.
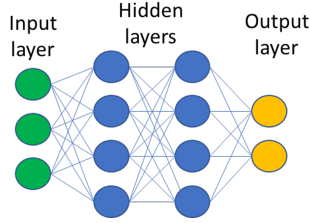

Figure 6: *Feed-forward neural network architecture*

The benefits of using ANNs also include not requiring *a priori* assumptions of the data used for training and not requiring weighting of initial inputs [9]. In practice, dimensionality reduction is often used to remove inputs to the model that are not independent and identically distributed (IID) or offer little influence to the overall training.

Training of ANNs use gradient-based optimization to update the weights that interconnect the nodes. Through a series of back propagation, the weights are individually modified in an iterative process. The training data is then run through the network again in order to measure the error again. Each complete cycle of training is called an epoch. There is no "one-size-fits-all" architecture and a key challenge of using machine learning tools is selecting an appropriate architecture based on the datasets available and the desired output [?].

This research uses datasets generated from RANS-CFD simulations on 61 different hull designs under various conditions defined by Froude number (Fn), leeway (β), and heel angle (ϕ) to train multi-layer neural networks in order to interpolate component forces under scenarios outside of the training set provided.

iii. Training set: Delft Wind Assist Series

A total set of 1,567 different RANS-CFD runs were prepared and executed over the period of 2016 and 2019 using the Numeca ISIS-CFD package. Vessel sailing performance for a range of Froude number (Fn), leeway (β), and heel angle (ϕ). The parameter space for hull geometry is indicated in Figure 7 and Table 1.

T/L Draft to length ratio

C_P Prismatic coefficient A_{Midship}/LBT

C_M Midship coefficient A_{Midship}/BT

The Delft Wind Assist series is a set of 60 hull forms developed by researchers at Delft University of Technology. The hull forms are in a systematic way so that the influence of significant form coefficients for sailing behavior may be isolated and studied. The series is set up to span a design space that is presently meaningful for the application of wind-assist propulsion, summarized in Table 1.

The DWA is composed of three sub-series's:

1st Series	Variations on the Ecoliner concept [19]
2nd Series	19th century clipper ships
3rd Series	Low-C_P ships (ferry, cruise, and ro-ro types)

III.   RESULTS

i.   Test Case

IV.   DISCUSSION

Reynolds-averaged Navier Stokes computational fluid dynamics (RANS-CFD) packages are often used during the development of performance predictions for commercial ships, requiring intensive computational resources and
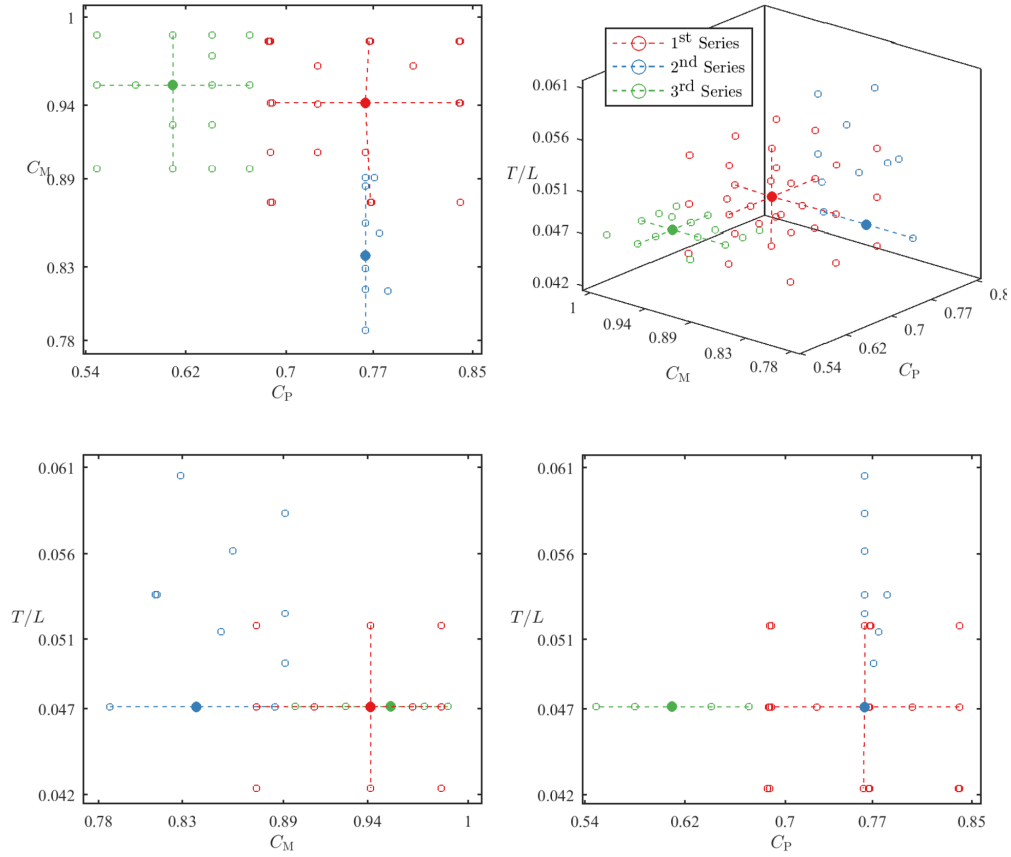
Figure 7: *Delft wind assist series, showing main parameter variations for T/L, C_P, and C_M*

complex software to generate results. Individual adjustments to parameters require discrete processing that may take hours to process. To expedite results under different hull designs, machine learning models were trained on RANS-CFD outputs to reproduce responses to different input values. The model successfully reproduced the RANS-CFD results with over 98% accuracy for 60 different hull variations and allowed for rapid estimation of results based on component force inputs. As a result, the different hulls can be quickly evaluated under different input conditions.

References

[1] Description of cartesius system. website. URL `https://userinfo.surfsara.nl/systems/cartesius`.

[2] A. R. Claughton and J. C. Oliver. Developments in hydrodynamic force models for velocity prediction programs. In *Conference on The Modern Yacht*. Royal Institute of Naval Architects, September 2003.

[3] G. B. Deng, E. Guilmineau, P. Queutey, and M. Visonneau. Ship flow simulations with the ISIS-CFD code. CFD Workshop Tokyo, CFD Workship Tokyo, 2005.

[4] G. B. Deng, P. Queutey, and M. Visonneau. A code verificaion exercise for

Table 2: *Network hyperparameters used to build the feed forward neural network*

Neural Network Parameter	Value
Hidden layers	2
Hidden layer nodes	30
Input and hidden layer activation function	sigmoid
Output activation function	tanh
learning rate (α_{lr})	0.002
Optimizer	Nesterov Adam
Loss Function	Mean Square Error
Dropout	0.2
Batches	100

the unstructured finite volume cfd solver ISIS-CFD. ECCOMAS-CFD, 2006.

[5] R. Duvigneau and M. Visonneau. On the role played by turbulence closures in hull shape optimization at model and full scale. *Journal of Marine Science and Technology*, 8:11–25, 2003.

[6] R. Eggers. Operational performance of wind assisted ships. In *10th Symposium on High-Performance Marine Vehicles (HIPER)*, Cortona, Italy, 2016.

[7] Brian S. Freeman, Graham Taylor, Bahram Gharabaghi, and Jesse Thé. Forecasting air quality time series using deep learning. *Journal of the Air & Waste Management Association*, 68(8):866–886, 2018. doi: 10.1080/10962247.2018.1459956.

[8] T. Fujiwara, G. Hearn, F. Kitamura, M. Ueno, and Y. Minami. Steady sailing performance of a hybrid-sail assisted bulk carrier. *Journal of Marine Science and Technology*, pages 131–146, 2005.

[9] M. W. Gardner and S. R. Dorling. Artificial neural networks (the multilayer perceptron)a review of applications in the atmospheric sciences. *Atmospheric Environment*, 32(1415):2627–2636, 1998. ISSN 1352-2310. doi: http://doi.org/10.1016/S1352-2310(97)00447-0.

[10] J. Gerritsma and J. A. Keuning. Sailing

Table 1: *Hydrostatics for hulls of the Delft Wind Assist Series (features of the ANN model)*

	C_{B}	C_{P}	C_{M}	C_{WP}	L/B	B/T	T/L	Deadrise
DWA (*N*=60)								
series max	0.827	0.840	0.988	0.925	8.44	3.54	0.061	0°
series min	0.493	0.549	0.787	0.747	6.00	2.16	0.042	0°
1st Series (*N*=33)								
Hull 1 (Parent)	0.719	0.764	0.942	0.883	7.67	2.77	0.047	0°
series max	0.827	0.840	0.984	0.925	8.44	3.42	0.052	0°
series min	0.601	0.686	0.874	0.832	6.90	2.29	0.042	0°
2nd Series (*N*=11)								
Hull 34 (Parent)	0.641	0.764	0.838	0.883	7.67	2.77	0.047	10°
series max	0.687	0.782	0.891	0.890	7.67	2.77	0.061	14°
series min	0.602	0.764	0.787	0.874	7.67	2.16	0.047	6°
3rd Series (*N*=15)								
Hull 45 (Parent)	0.582	0.610	0.954	0.805	6.00	3.54	0.047	0°
series max	0.663	0.671	0.988	0.841	6.00	3.54	0.047	0°
series min	0.493	0.549	0.897	0.747	6.00	3.54	0.047	0°

Table 3: *Main particulars for Panamax test case.*

LOA [m]	290
Beam [m]	32
Draft [m]	24
DWT tonnage [ton]	80 000
Airdraft [m]	40
Number of rotors	5
Rotor height [m]	30
Block Coeff. C_B	0.83
Prismatic Coeff. C_P	0.835
Hull aspect ratio T/L	0.083
Sail area ratio $\frac{SA}{\Delta^{2/3}}$	0.404

Table 4: *Comparison error for Panamax test vessel maneuvering coefficients.*

	RANS-CFD	N-N Model	% diff
Fn =0.126			
$X_{\beta\beta}$	0.116 09		
X_{ϕ}	0.007 92		
Y_{β}	0.0589		
$Y_{\beta\beta\beta}$	2.014		
Y_{ϕ}	0.097		
N_{β}	0.144		
N_{ϕ}	0.052		
Fn =0.168			
$X_{\beta\beta}$	0.129		
X_{ϕ}	0.008 27		
Y_{β}	0.0692		
$Y_{\beta\beta\beta}$	2.0		
Y_{ϕ}	0.119		
N_{β}	0.144		
N_{ϕ}	0.059		
Fn =0.21			
$X_{\beta\beta}$	0.133		
X_{ϕ}	0.009 33		
Y_{β}	0.0770		
$Y_{\beta\beta\beta}$	2.10		
Y_{ϕ}	0.152		
N_{β}	0.147		
N_{ϕ}	0.072		

yacht performance in calm water and in waves. In *HISWA Symposiumon Yacht Design and Yacht Construction*, pages 233–245, Amsterdam, 1992.

[11] J. Gerritsma, J. A. Keuning, and A. Versluis. *Sailing yacht performance in calm water and in waves*. 1993.

[12] Ian Goodfellow, Yoshua Bengio, and Aaron Courville. *Deep Learning*. MIT Press, 2016. ISBN 9780262035613. URL `http://www.deeplearningbook.org`. Accessed 29 Jan 2018.

[13] S. F. Hoerner. *Fluid Dynamic Lift - Practical Information on Aerodynamic and Hydrodynamic Lift*. Mrs. Liselotte A. Hoerner, Vancouver, 1985.

[14] S. Inoue, H. Masayoshi, and K. Katsuro. Hydrodynamic derivatives and ship manoeuvering. *International Shipbuilding Progress*, 1981.

[15] W. Jacobs. Estimation of stability derivatives and indices of various ship forms, and comparison with experimental results. *Journal of Ship Research*, pages 135–163, 1966.

[16] R. T. Jones. Properties of low-aspect ratio pointed wings at speeds below and above the speed of sound. Technical Report 835, NACA, 1946.

[17] J. A. Keuning and U. B. Sonnenberg. Approximation of the hydrodynamic forces on a sailing yacht based on the 'delft systematic yacht hull series'. In *HISWA Symposiumon Yacht Design and Yacht Construction*, pages 99–152, 1998.

[18] M. M. Munk. Remarks on the pressure distribution over the surface of an ellipsoid moving translationally through a perfect fluid. Technical report, NACA, 1924.

[19] Dykstra NA. Ecoliner, 2010.

[20] P. Naaijen, W. Shi, and J. Kherian. Assessing the fuel savings by using auxiliary wind propulsion from traction kites. *RINA - Ship Design and Operation for Environmental Sustainability - Papers*, pages 27–37, 2010.

[21] Numeca Inc. ISIS theoretical manual. Technical report, Numeca International.

[22] L. Prandtl. Tragflügeltheorie. *Königliche Gesellschaft der Wissenschaften*.

[23] P. Queutey and M. Visonneau. An interface capturing method for free-surface hydrodynamic flows. *Computers and Fluids*, 36:1481–1510, 2007.

[24] Amel Sifaoui, Afef Abdelkrim, and Mohamed Benrejeb. On the use of neural network as a universal approximator. *International Journal of Sciences*, 2:386–399, 08 2008.

[25] Sho Sonoda and Noboru Murata. Neural network with unbounded activation functions is universal approximator. *Applied and Computational Harmonic Analysis*, 43(2):233 – 268, 2017. ISSN 1063-5203. doi: https://doi.org/10.1016/j.acha.2015.12.005. URL `http://www.sciencedirect.com/science/article/pii/S1063520315001748`.

[26] Tahsin Tezdogan, Yigit Kemal Demirel, Paula Kellett, Mahdi Khorasanchi, Atilla Incecik, and Osman Turan. Full-scale unsteady rans cfd simulations of ship behaviour and performance in head seas due to slow steaming. *Ocean Engineering*, 97:186 – 206, 2015. ISSN 0029-8018. doi: https://doi.org/10.1016/j.oceaneng.2015.01.011. URL `http://www.sciencedirect.com/science/article/pii/S0029801815000190`.

[27] S. L. Toxopeus. Practical application of viscous-flow calculations for the simulation of manoeuvering ships. *PhD Thesis*, 2011.

[28] Michael Traut, Paul Gilbert, Conor Walsh, Alice Bows, Antonio Filippone, Peter Stansby, and Ruth Wood. Propulsive power contribution of a kite and a Flettner rotor on selected shipping routes. *Applied Energy*, 113:362–372, 2014. doi: 10.1016/j.apenergy.2013.07.026.

[29] S. Tsakonas. Effect of appendage and hull form on hydrodynamic coefficients of surface ships. Technical report, Hoboken, NJ, 1959.

[30] N.J. van der Kolk, I. Akkerman, J. A. Keuning, and R.H.M. HUuijsmans. Part 2: Simulation methodology and numerical uncertainty for rans-cfd for the hydrodynamics of wind-assisted ships operating at leeway angles. Manuscript accepted for publication.

[31] van der Kolk N. J., J. A. Keuning, and R. H. M. Huijsmans. Part 1: Experimental validation of a RANS-CFD methodology for the hydrodynamics of wind-assisted ships operating at leeway angles. *Ocean Engineering*, 178:375387, 2018. doi: 10.1016/j.oceaneng.2018.12.041.